3388–3398 *Nucleic Acids Research, 2010, Vol. 38, No. 10* *Published online 27 January 2010*
doi:10.1093/nar/gkq020

NMR structure and dynamics of the Specifier Loop domain from the *Bacillus subtilis tyrS* T box leader RNA

Jiachen Wang[1], Tina M. Henkin[2] and Edward P. Nikonowicz*

[1]Department of Biochemistry and Cell Biology, Rice University, Houston, TX 77251-1892 and [2]Department of Microbiology and Center for RNA Biology, The Ohio State University, Columbus, OH 43210, USA

Received December 3, 2009; Revised January 7, 2010; Accepted January 8, 2010

ABSTRACT

Gram-positive bacteria utilize a tRNA-responsive transcription antitermination mechanism, designated the T box system, to regulate expression of many amino acid biosynthetic and aminoacyl-tRNA synthetase genes. The RNA transcripts of genes controlled by this mechanism contain 5′ untranslated regions, or leader RNAs, that specifically bind cognate tRNA molecules through pairing of nucleotides in the tRNA anticodon loop with nucleotides in the Specifier Loop domain of the leader RNA. We have determined the solution structure of the Specifier Loop domain of the *tyrS* leader RNA from *Bacillus subtilis*. Fifty percent of the nucleotides in the Specifier Loop domain adopt a loop E motif. The Specifier Sequence nucleotides, which pair with the tRNA anticodon, stack with their Watson–Crick edges rotated toward the minor groove and exhibit only modest flexibility. We also show that a Specifier Loop domain mutation that impairs the function of the *B. subtilis glyQS* T box RNA disrupts the *tyrS* loop E motif. Our results suggest a mechanism for tRNA–Specifier Loop binding in which the phosphate backbone kink created by the loop E motif causes the Specifier Sequence bases to rotate toward the minor groove, which increases accessibility for pairing with bases in the anticodon loop of tRNA.

INTRODUCTION

The expression of many aminoacyl-tRNA synthetase genes and genes involved in amino acid metabolism and uptake in Gram-positive bacteria is regulated at the level of transcription attenuation by the T box riboswitch, an RNA element in the 5′ untranslated (or leader) region of the gene (1,2). The expression of genes in this family is determined by the relative levels of charged and uncharged tRNAs in the cell, with each gene in the family responding individually to a specific tRNA species. If the corresponding tRNA is highly aminoacylated, a transcriptional attenuator in the leader region is active, and the gene is not expressed. Readthrough of the termination site is dependent on binding of uncharged tRNA to the T box element, which is 200–300 nt in length and contains several conserved primary and secondary structure elements, including three helices (Stems I, II and III), the Stem IIA/B pseudoknot and the terminator and antiterminator structures (Figure 1A). The secondary structures of the terminator and antiterminator helices are mutually exclusive and the terminator helix is thermodynamically more favorable (3). Stabilization of the antiterminator helix, and subsequent transcriptional readthrough, is accomplished by pairing of the four 3′ terminal nucleotides of the tRNA molecule with residues in a 7-nt bulge of the antiterminator helix (4).

Specific tRNA recognition is dependent primarily on the identity of three nucleotides, the Specifier Sequence, within the Specifier Loop domain, a conserved internal loop of variable size located in Stem I (3,5). The Specifier Sequence nucleotides are complementary to the anticodon nucleotides of the cognate tRNA. Changes in the Specifier Sequence can in some cases result in a switch in the specificity of the T box riboswitch to allow recognition of a new tRNA (3,5,6). The residue 3′ to the Specifier Sequence is conserved as a purine, and pairs with the conserved U at position 33 in tRNA, 5′ to the anticodon (7). The functional importance of these tRNA–leader RNA interactions have been demonstrated for the *Bacillus subtilis tyrS* and *glyQS* leader RNAs (3,8) and reproduced *in vitro* using a purified transcription assay and the *glyQS* leader RNA (9,7). In addition, interaction between *glyQS* Specifier Loop domain and $tRNA^{Gly}$ anticodon stem–loop was demonstrated with fluorescence assays (10).

In addition to the overall secondary structure and nucleotide conservation of T box leader RNAs (3), a

*To whom correspondence should be addressed. Tel: +1 713 348 4912; Fax: +1 713 348 5154; Email: edn@rice.edu

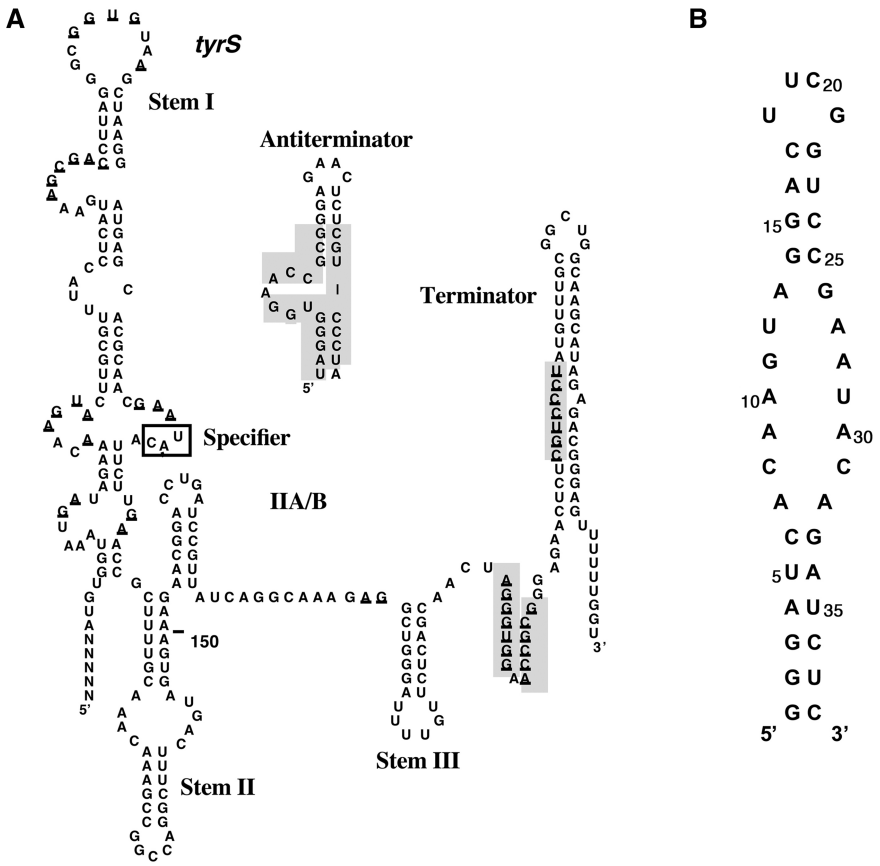

Figure 1. Sequence and proposed secondary structures of (**A**) the leader RNA of the *B. subtilis tyrS* gene and (**B**) the 38-nt RNA molecule, $tyrS_{SD}$, corresponding to the Specifier Loop domain of the *tyrS* leader RNA.

loop E (or S-turn) motif is predicted to form in the Specifier Loop (11). The loop E motif is a common RNA structural element found in many RNAs including ribosomal RNAs (12–14), the hairpin ribozyme (15), and the nucleolin-recognition element in eukaryotes (16,17). The sequences and structures of these motifs are very similar among different RNAs and feature a group of three non-canonical base pairs (18). This motif frequently is located proximal to multi-helix junctions and has crucial roles in protein-binding sites and in mediating RNA–RNA interactions (14). The high conservation of this motif within the Specifier Loop suggests an important role in leader RNA function, including tRNA binding.

The Specifier Loop domain of the *B. subtilis tyrS* leader RNA is an internal loop of 14 nt, including the 4 nt that pair with the $tRNA^{Tyr}$ anticodon loop, flanked by two short helices. We have used heteronuclear nuclear magnetic resonance (NMR) spectroscopy to determine the solution structure and dynamics of this domain. Our results confirm the presence of the predicted loop E structural element within the internal loop, adjacent to the Specifier Sequence. We also show that a mutation within the loop E nucleotides that leads to loss of function in the context of the *B. subtilis glyQS* T box leader (Green,N.J., Grundy,F.J. and Henkin,T.M., unpublished data), destabilizes the motif, but does not significantly alter the conformation of the internal loop, confirming the importance of this motif for proper function.

MATERIALS AND METHODS

Materials

All enzymes were purchased from Sigma Chemical (St. Louis, MO, USA) except for T7 RNA polymerase, which was prepared as described (19). Deoxyribonuclease I type II, pyruvate kinase, adenylate kinase and nucleotide monophosphate kinase were obtained as powders, dissolved in 15% glycerol, 1 mM dithiothreitol and 10 mM Tris–HCl, pH 7.4, and stored at –20°C. Guanylate kinase and nuclease P1 were obtained as solutions and stored at –20°C. Unlabeled 5′ nucleoside triphosphates (5′-NTPs) were purchased from Sigma, phosphoenolpyruvate (potassium salt) was purchased from Bachem, and 99% [^{15}N]-ammonium sulfate and 99% [^{13}C]-glucose were purchased from Spectra Stable Isotopes (Branchburg, NJ, USA).

Preparation of RNA samples

The RNA sequence depicted in Figure 1B was prepared by *in vitro* transcription with T7 RNA polymerase using a synthetic DNA template (20) and either unlabeled

5′-NTPs or $^{13}C/^{15}N$ -labeled 5′-NTPs as previously described (21). The RNA molecules were purified using 20% (w/v) preparative polyacrylamide gels, electroeluted (Schleicher & Schuell), and precipitated with ethanol. The purified RNA molecules were resuspended in 1.0 M KCl, 20 mM KPi, pH 6.8 and 2.0 mM EDTA and extensively dialyzed against 10 mM KCl, 5 mM KPi, pH 6.7 and 0.02 mM EDTA using a Centricon-3 concentrator (Millipore, Bedford, MA, USA). All RNA samples were concentrated to a volume of 320 µl, lyophilized to a powder, and either resuspended in 90% H_2O/10% D_2O or 99.96% D_2O. The samples were then heated to 80°C for 60 s and snap-cooled on ice. The sample concentrations varied between 120 and 180 A_{260} O.D. in 320 µl (~1.5–2.5 mM). Partial alignment of $^{13}C/^{15}N$-labeled RNA for residual dipolar coupling measurements was achieved by adding RNA to concentrated Pf1 filamentous phage in 99.96% D_2O NMR buffer, yielding final concentrations of 19 mg/ml Pf1 and 0.35 mM RNA. The degree of alignment was quantified using the quadrupole splitting of the ^2H_2O resonance (22).

NMR spectroscopy

All spectra were acquired on a Varian Inova 500-MHz spectrometer equipped with a ^1H–(^{13}C, ^{15}N, ^{31}P) probe and Inova 600 and 800-MHz spectrometers equipped with cryogenically cooled ^1H–(^{13}C, ^{15}N) probes. Solvent suppression for ^1H homonuclear spectra collected in 90% H_2O was achieved using the WATERGATE scheme. Typically, the data points were extended by 25% using linear prediction for the indirectly detected dimensions. NMR spectra were processed and analyzed using Felix 2007 (Felix NMR Inc., San Diego, CA, USA).

Two-dimensional (2D) ^{13}C-^1H HSQC spectra were collected to identify ^{13}C-^1H chemical shift correlations. Sugar spin systems were assigned using 3D HCCH-TOCSY (16 ms and 24 ms DIPSI-3 spin lock) experiments collected in D_2O. A 3D HCCH-TOCSY (56 ms DIPSI-3 spin lock) was collected to establish the intra-base H2-C2-C8-H8 correlations in adenine residues. A 3D HCN experiment (23) was used to identify intra-residue base–ribose correlations.

Sequential assignments and distance constraints for the non-exchangeable resonances were derived at 28°C from 2D ^1H -^1H nuclear Overhauser effect spectroscopy (NOESY) spectra (τ_m = 120, 160 and 360 ms) and 3D ^{13}C-edited NOESY spectra (τ_m = 120 and 360 ms). Pyrimidine C2 and C4 resonances were assigned from H6-C2 and H5-C4 correlations using 2D H(CN)C and 2D CCH-COSY experiments. 2D ^{15}N-^1H HSQC spectra optimized for 2-bond HN couplings were collected to identify purine N7 and adenine N1 and N3 resonances. For the exchangeable resonances, 2D ^{15}N-^1H HSQC spectra were collected to identify ^{15}N-^1H chemical shift correlations. 2D NOESY spectra (τ_m = 180 and 400 ms) were acquired in H_2O and at 12°C to obtain distance restraints involving exchangeable protons.

^1H-^{13}C residual dipolar coupling constants (RDCs) were determined from the measured frequency difference between corresponding proton doublets in HSQC spectra acquired for isotropic and partially aligned samples. Thirty RDC values from base CH bond vectors and 16 from ribose 1′ CH vectors were obtained in this manner. The axial and rhombic terms were determined within Xplor-NIH using an extensive grid search (24), and yielded values of D_{aH} = 31.67 and R_{hH} = 0.19.

$^3J_{HH}$ coupling constants were estimated from DQF-COSY experiments. $^3J_{C\text{-}P}$ coupling constants were determined using the ^{13}C-^1H ct-HSQC spin-echo difference method. $^3J_{P\text{-}H}$ couplings were estimated using ^{31}P-^1H HetCor experiments.

^{13}C $T_{1\rho}$ relaxation times were measured using 2D ^{13}C-^1H ct-HSQC-based experiments optimized for C2, for C1′ and for C6 and C8 resonances. A 2.1-kHz ^{13}C spin-lock field was used with delays of 5, 10, 15, 20, 30, 40, 50, 60, 70, 90 and 120 ms. The 5-ms experiment was collected twice to provide an estimate of the error of the measured intensities. The ^{13}C-^1H cross-peak volumes were fit to a single exponential decay.

Distance and torsion angle constraints

Interproton distance estimates were obtained from cross-peak intensities in 2D NOESY and 3D ^{13}C-edited NOESY spectra. Cross-peak intensities were calibrated using the pyrimidine H5–H6 fixed distance of 2.54 Å. NOE cross-peak intensities were classified into five categories assigned upper distance bounds of 3.0, 4.0, 5.0, 6.0 or 7.0 Å and a common lower bound of 1.8 Å. Base pairs were identified by direct detection of hydrogen bonds (25) or by observation of strong G•C NH–NH_2 or A•U H2–NH NOEs. Hydrogen bond distances restraints and planarity constraints were introduced for residues that form base pairs.

Ribose ring pucker and backbone dihedral constraints were derived from $^3J_{HH}$, $^3J_{HP}$ and $^3J_{CP}$ couplings (26). Ribose rings with $^3J_{H1'\text{-}H2'} > 7$ Hz and with C3′ and C4′ resonances between 76–80 and 85–86 p.p.m., respectively, were constrained to C2′-*endo*. Residues with $^3J_{H1'\text{-}H2'} < 5$ Hz and couplings were constrained to C3′-*endo*. Residues with intermediate $^3J_{H1'\text{-}H2'}$ couplings were left unconstrained. For stem residues 1–6 and 33–38, γ was constrained to the gauche$^+$ conformation (60 ± 30°) (26); γ was left unconstrained for all other residues. For stem residues, β was constrained to the *trans* conformation (170 ± 40°). β was loosely constrained to the *trans* conformation (160 ± 50°) for internal loop residues except G_{11} and A_{27} that were constrained loosely to gauche$^+$ (80 ± 50°) as determined from examination of loop E containing crystal structures (27,28). ε was constrained to exclude the gauche$^+$ conformation (–150 ± 50°) for residues with $^3J_{P\text{-}H3'} > 5$ Hz or $^3J_{P\text{-}C2'} > 5$ Hz. α and ζ were constrained to –70 ± 30° for the stem residues and were constrained to exclude the *trans* conformation (0 ± 120°) for residues 7–14 and 25–32 based on the absence of down-field shifted ^{31}P resonances (29).

Structure refinement

Structure refinement was carried out with simulated annealing and restrained molecular dynamics (rMD) calculations were performed using Xplor-NIH v2.19 (24).

Starting coordinates for the $tyrS_{SD}$ model were generated using Insight II (Accelrys, San Diego, CA, USA) and were based on standard A-form helical geometry. The structure calculations were performed in two stages. Beginning with the energy-minimized starting coordinates, 100 structures were generated during the first round of structure calculation by 80 ps of rMD at 1200 K with hydrogen bond, NOE-derived distance and base-pairing restraints. The system then was cooled to 25 K in 47 cycles of rMD corresponding to a total of 12 ps. During this stage, RDC constraints and repulsive van der Waals forces were introduced into the system and the SANI force const0raint used for RDCs was gradually increased from 0.010 kcal mol^{-1} Hz^{-2} to 1.000 kcal mol^{-1} Hz^{-2}. Other force constants used for the calculations were increased—from 2 kcal mol^{-1} Å^{-2} to 30 kcal mol^{-1} Å^{-2} for the NOE and from 2 kcal mol^{-1} rad^{-2} to 30 kcal mol^{-1} rad^{-2} for the dihedral angle constraints. Once the temperature reached the target, each structure was then subjected to another round of constrained minimization (30). Ten structures were selected for the final refinement. The criteria for final structure selection included lowest energies, fewest constraint violations and fewest predicted unobserved NOEs (^{1}H pairs <3.5 Å apart, but no corresponding cross-peak in the NOE spectra). A second round of rMD was performed on these structures using protocols similar to those used in the first round of structure calculation. The major difference was the starting temperature of 300 K followed by cooling to 25 K over 28 ps of rMD. The 10 refined structures were analyzed using Xplor-NIH and Insight II.

RESULTS

The RNA molecule used in this study, $tyrS_{SD}$ (Figure 1B), corresponds to the Specifier Loop from Stem I of *B. subtilis tyrS* leader RNA. Cross-peaks in the NH ^{15}N-^{1}H HSQC spectrum and the resonance linewidths are consistent with the predicted secondary structure, and the NH spectra at low concentration (5 μM) and high concentration (1.8 mM) are nearly identical, supporting the prediction that the RNA is monomeric. The addition of Mg^{2+} or the reduction of pH from 6.8 to 5.5 caused slight broadening of a few NH resonances, but did not lead to the appearance of new peaks.

Chemical-shift assignments

The sequence-specific resonance assignment of $tyrS_{SD}$ was accomplished using ^{1}H-^{1}H NOESY and 2D and 3D heteronuclear experiments. The NH resonances were assigned using the NOE connectivities between NH proton resonances of neighboring base pairs. These connectivities are continuous in the lower helix from G_2 to G_{33} and the upper helix from G_{14} to G_{21}. The cytidine and adenine NH_2 resonances were assigned using NOESY and HNCCH experiments (31). Additional weak NH resonances are present in the 1D ^{1}H spectrum between 10.5 and 11.8 p.p.m., but cannot be uniquely assigned to U_{12}, U_{19}, U_{29}, G_1, G_{11} or G_{26}.

The non-exchangeable ^{1}H and ^{13}C resonances of $tyrS_{SD}$ were assigned using standard heteronuclear techniques (32,33). Most of the base and ribose 1′ ^{1}H-^{13}C correlations are resolved, with four of the base resonances (A_{13}, G_{14} and G_{26} H8-C8 and A_{13} H2-C2) having spectral characteristics indicative of intermediate exchange (Figure 2A). All residues except U_{12}, A_{13} and G_{14} yielded base–ribose correlations in 3D HCN spectra, and 37 of the ribose spin systems were identified using 3D HCCH-TOCSY experiments (G_1 was only partially labeled).

Assignments for the non-exchangeable resonances were made using 2D NOESY (Figure 2B) and 3D ^{13}C-edited NOESY experiments to identify sequential H6/8-H1′ NOE connectivities (32). The sequential H6/8-H1′ NOE connectivities are continuous in the 180-ms NOESY spectrum except at steps A_{10}–G_{11} and G_{11}–U_{12}. However, G_{11}H8–U_{12}H6 and G_{11}H4′–U_{12}H6 cross-peaks are present in the spectrum. Interestingly, i to i+2 NOE cross-peaks between A_{10}H1′/H2′ and U_{12}H6 are observed (Figure 2B) and suggest that the G_{11} base bulges from the strand. The chemical shifts of G_{14}H1′ (4.25 p.p.m.) and G_{11}H4′ (5.85 p.p.m.) are unusual and are discussed below.

Most inter-nucleotide ^{31}P resonances are dispersed between –3.4 and –5.1 p.p.m., but the G_{21}pG_{22} resonance has a chemical shift of –2.19 p.p.m. as previously noted for the UNCG tetraloop motif (34). Several ^{31}P resonances could be assigned using the HCP experiment (35) or the H8/6-P and H1′-P correlations from 2D ^{31}P-^{1}H hetero-TOCSY-NOESY spectra (36). The chemical shifts for $tyrS_{SD}$ are listed in Supplementary Table S1.

Structure of the $tyrS_{SD}$ molecule

The structure of $tyrS_{SD}$ was calculated using a restrained molecular dynamics routine. The calculations used a total of 296 conformationally restrictive distance constraints, 189 dihedral angle constraints and 46 RDC constraints (Table 1) to produce 10 converged structures (Figure 3). The converged structures had an average of 5.8 distance constraint violations between 0.3 and 0.6 Å that were randomly distributed throughout the hairpins. None of the converged structures had NOE constraint violations >0.6 Å. The heavy atoms of the converged structures superimpose on the average structure with an average root mean square deviation (RMSD) of 1.25 Å. The local RMSDs for the loop (A_7–A_{13} and G_{26}–A_{32}) and stems are 0.54 Å and 1.22 Å, respectively.

The abundance of constraints for the internal loop and flanking stem nucleotides (residues C_6–G_{14} and C_{25}–G_{33}) defines the conformation of these nucleotides with good precision (0.60 Å rmsd) (Figure 3B and Table 1). The ribose ring puckers of several residues in the internal loop adopt non-A-form, C3′-*endo*, conformations. Residues A_9, A_{10} and A_{32} adopt C2′-*endo* ring puckers and residues G_{11}, A_{13}, G_{26} and A_{28} exhibit conformations intermediate between C2′-*endo* and C3′-*endo*.

The $tyrS_{SD}$ Specifier Loop domain contains a loop E motif. The nucleotide sequence within the $tyrS_{SD}$ RNA corresponding to the loop E motif is similar to that found in several eukaryotic 5S rRNAs (37) and the

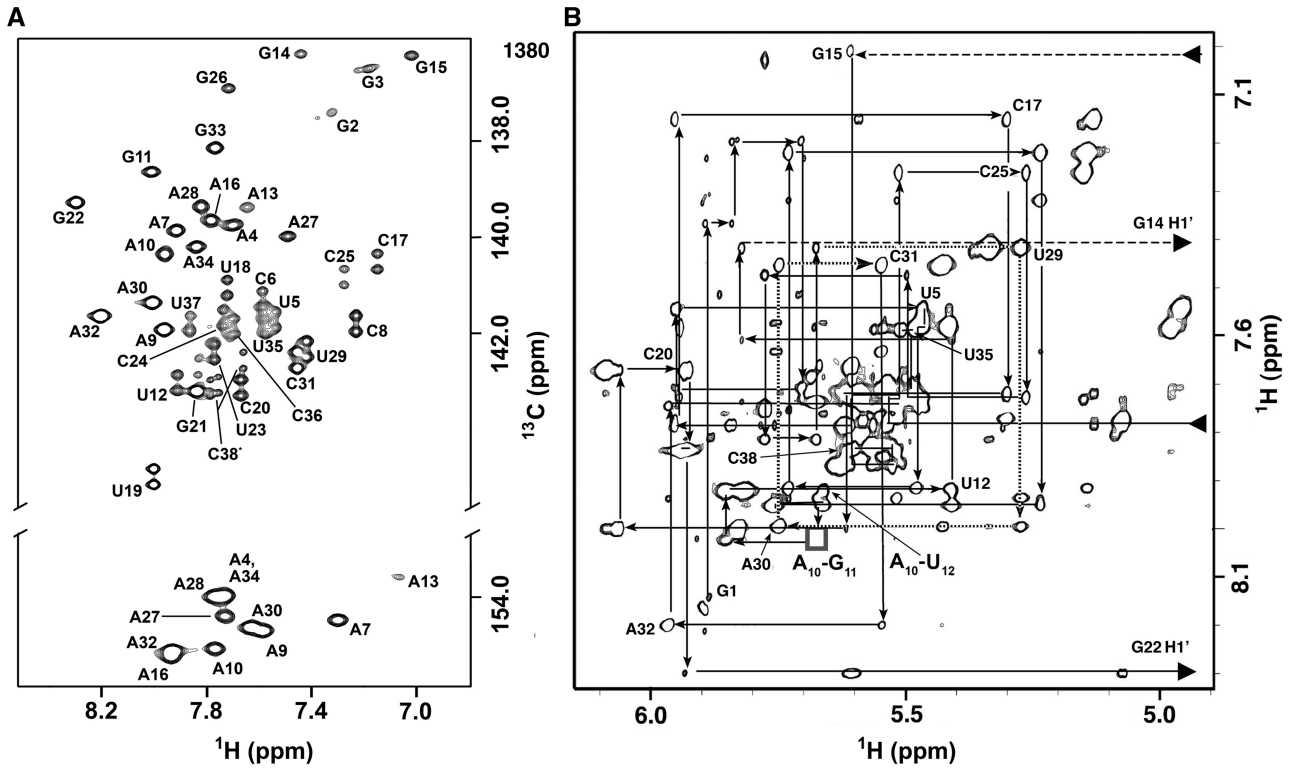

Figure 2. (A) Two-dimensional ^{13}C-^{1}H HSQC spectrum of the base C6/8 and C2 regions of $tyrS_{SD}$ RNA molecule. The sequence-specific resonance assignments are shown. The A_{13} C2H2 cross-peak is significantly weakened by chemical exchange. The *in vitro* transcription reaction was primed with unlabeled 5′-GMP, therefore the G_1 C8H8 does not appear in this spectrum. (**B**) Sequential connectivities through the base-1′ region of the 220-ms mixing time two-dimensional NOE spectrum. The dotted lines trace the connectivities among the specifier codon nucleotides U_{29}–A_{31}. The sequential connectivity is disrupted between steps A_{10}–G_{11} (gray box). The H1′ resonances of G_{14} and G_{22} are shifted upfield to 4.25 and 4.42 p.p.m., respectively. These chemical shifts are characteristic of the nucleotides flanking the 3′ side of the adenine of a sheared G–A base pair and the guanine of a UNCG tetraloop (59). See also Supplementary Table S1.

hairpin ribozyme (15,38). The core of this element typically contains three nonstandard base–base interactions, a sheared A–G pair, a U–A trans-Hoogsteen interaction and a parallel A–A base pair, that stack on one another (13). In some cases, a bulged G or C nucleotide is present between the non-canonical U–A and A–A interactions. The spectral data indicate that the loop E motif structure is present but adopts a more open conformation than is found in other contexts. A characteristic spectral signature of the sheared A–G pair is an upfield shift of the H1′ resonance of the residue 3′ to the A (13,17,39). This H1′ resonance shift is observed for G_{14} and is consistent with a sheared A_{13}–G_{26} orientation. The sheared A–G base pair forms two hydrogen bonds, $AN6H_2$–GN3 and AN7–$GN2H_2$ (Figure 4), and the A_{13} N7 and N6 ^{15}N chemical shifts provide additional support for the A_{13}–G_{26} interaction. The trans-Hoogsteen U–A interaction adjacent to the sheared A–G pair also produces a very unusual spectral feature, an $A_{10}H8$–$U_{12}H1'$ NOE cross-peak. The trans-Hoogsteen U–A arrangement rotates the uridine ribose ring so that the H1′ is repositioned proximal to the 5′ (i-2) residue rather than the 3′ (i + 1) residue. The U–A interaction involves hydrogen bonds between UO2 and $AN6H_2$ and UN3H and AN7 (14). The U_{12}N3H resonance is exchange-broadened and could not be observed, indicative of a weak hydrogen bond or solvent-accessible U_{12}N3H. Adjacent to the trans-Hoogstein base pair is a parallel A–A interaction (Figure 4). The parallel A–A base pair is facilitated by an S-turn in the phosphate backbone and stabilized by two symmetric $N6H_2$–N7 inter-base hydrogen bonds (14,28). The ^{15}N chemical shifts are consistent with the $A_{28}N6H_2$–$A_{10}N7$ hydrogen bond, but the chemical shifts do not support the second (symmetric) interaction (Supplementary Table S1; Figure 4). The G_{11} base is bulged and its conformation is supported by NOE data. Several i, i + 2 NOE cross-peaks connect A_{10} with U_{12} and no inter-residue NOE cross-peaks are observed between G_{11} and the A_{10} ribose. These NOE cross-peaks indicate stacking of the A_{10} and U_{12} bases. Efforts to confirm the predicted hydrogen bonds via through-bond correlation experiments (25) were unsuccessful. This result is consistent with the ^{15}N chemical-shift data that suggest weak hydrogen bonds.

A hallmark of the loop E motif is the turn in the phosphate backbone 5′ to the bulged nucleotide (between A_{10} and G_{11}) (28). This turn permits the parallel A–A interaction without the adenine residues adopting the *syn* orientation about the glycosidic bond. The turn itself is accommodated by the flipping of the ribose moiety of one of the adenine residues relative to other ribose groups along the phosphate backbone. This ribose

Table 1. Summary of experimental distance and dihedral angle constraints and refinement statistics for $tyrS_{SD}$

Constraint	$tyrS_{SD}$
NOE distance constraints	
Intra-residue[a]	87
Inter-residue	135
Mean number per residue	16
NOE constraints by category	
Very strong (1.8–3.0 Å)	34
Strong (1.8–4.0 Å)	180
Medium (1.8–5.0 Å)	215
Weak (1.8–6.0 Å)	117
Very weak (1.8–7.0 Å)	24
Base pair constraints	
Total	32
Dihedral angle constraints	
Ribose ring[b]	104
Backbone	189
Mean number per residue	7.7
Residual dipolar coupling constraints	
Base CH	30
Ribose 1′ CH	16
Violations	
Average distance constraints > 0.5 Å[c]	5.8
Average dihedral constraints > 0.5°[d]	1.6
RMSD from ideal geometry[e]	
Heavy atoms (Å)	1.24
Backbone atoms (Å)	1.27

[a]Only conformationally restrictive constraints are included.
[b]Three torsion angles within each ribose ring were used to constrain the ring to either the C2′-endo or C3′-endo conformation; the ring pucker of residues G_{11}, A_{13}, G_{26} and A_{28} were not constrained.
[c]A distance violation of 0.5 Å corresponds to 5.0 kcal energy penalty.
[d]A dihedral angle violation of 0.5° corresponds to 0.05 kcal energy penalty.
[e]Calculated against the minimized average structure.

orientation is supported by a characteristic NOE pattern (13,17) that includes weak intensity A_{10} H4′–U_{12} H6 and A_{10} H4′–U_{12} H5 cross-peaks and moderate intensity A_{10} H4′–U_{12} H1′ and A_{10} H8–U_{12} H1′ cross-peaks.

The Specifier Sequence bases are stacked. The remaining nucleotides in the Specifier Loop domain are asymmetrically distributed, four on the Specifier Sequence strand and three on the opposite strand (Figures 3 and 5). The calculated structures show intra-strand stacking and slight rotation of the Specifier Sequence (U_{29}, A_{30} and C_{31}) bases toward the minor groove. A_{32} also is rotated toward the minor groove, but stacks with G_{33} of the lower helix. These structures are consistent with the experimental data, i.e. base–base and 'standard' base–ribose NOEs and $^{15}N/^{13}C$ chemical shifts characteristic of unpaired bases. This conformation may facilitate pairing of the Specifier Sequence bases with the tRNA anticodon loop through the ordered presentation of the Watson–Crick edges of the bases.

Localization of metal ion binding sites in the $tyrS_{SD}$ RNA

Metal ions play important roles in RNA structure and function by facilitating RNA folding, stabilizing tertiary structure and participating directly in catalysis. Mg^{2+} is crucial for the correct folding of *glyQS* leader RNA (7), but the specific structural changes and exact sites of coordination associated with Mg^{2+} binding are not known.

The effects of Mg^{2+} on different RNAs that contain loop E motifs are variable. NMR spectra show that the loop E motif in eukaryotic 5S rRNA is stabilized by Mg^{2+} (40), but spectra of the same motif sequence located in the sNRE and the hairpin ribozyme are unaffected by Mg^{2+} (41–43). In addition, no metal ions are associated with the loop E motif in the crystal structure of the sarcin/ricin loop of 5S rRNA (44).

The NH and NH_2 chemical-shift perturbations by Mg^{2+} are limited to the G_2–U_{37} NH resonances in $tyrS_{SD}$. However, the chemical shifts of several CH base resonances are altered by up to 0.15 p.p.m. (Supplementary Figure S1). These include the base C8–H8 and C6–H6 resonances of loop residues G_{33}, C_8, A_{27}, A_9 and C_{31} and adenine C2–H2 resonances A_{13}, A_7, A_9 and A_{32}. The intensity of the A_{13} H8–C8 resonance increases, but the G_{11} H8–C8 resonance broadens. Significantly, the pattern and intensities of NOE cross-peaks of the Mg^{2+}-free sample are largely preserved upon addition of Mg^{2+}, indicating little or no structural impact.

^{13}C Relaxation measurements

The reorientation of a ^{13}C-^{1}H bond vector on the picosecond timescale can be assessed through its carbon $T_{1\rho}$ relaxation: the longer the relaxation time, the more mobile the ^{13}C-^{1}H pair. The $T_{1\rho}$ relaxation times for the base C6 and C8 and ribose C1′ positions of $tyrS_{SD}$ were measured. Cross-peak overlap and chemical exchange prevented accurate measurement of a few adenine C2 nuclei, pyrimidine C6 and several C1′ nuclei. The majority of base resonances from internal loop residues exhibited relaxation times between 40 and 50 ms, which are comparable to stem region nucleotides. However, the $T_{1\rho}$ values for nucleotides A_{10}, G_{26}, A_{27} and A_{28} within the loop E motif and the proximal stem nucleotides G_{14}, and C_{25} were increased by 20%, indicative of increased mobility. Chemical exchange is dominant among the base resonances of G_{11} U_{12} and A_{13} and prevents accurate $T_{1\rho}$ measurements for these residues. A similar pattern is not exhibited by the C1′ nuclei. Only the A_9, A_{10}, A_{28} and A_{30} residues from the internal loop have relaxation times 30–50% longer than other residues in the internal loop and the stems. The increased relaxation times of nucleotide base resonances and exchange broadening for residues in the region of the loop E motif are consistent with a structural element that is moderately rigid. The addition of Mg^{2+} did not significantly alter the relaxation profile of the $tyrS_{SD}$ RNA.

DISCUSSION

The T-box mechanism for regulation of amino acid-related genes is widely utilized in Gram-positive bacteria. Extensive mutagenesis studies of the leader RNA sequence have defined sequence requirements for tRNA binding in the 5′ and 3′ regions of the leader RNA (4–6,11,45).

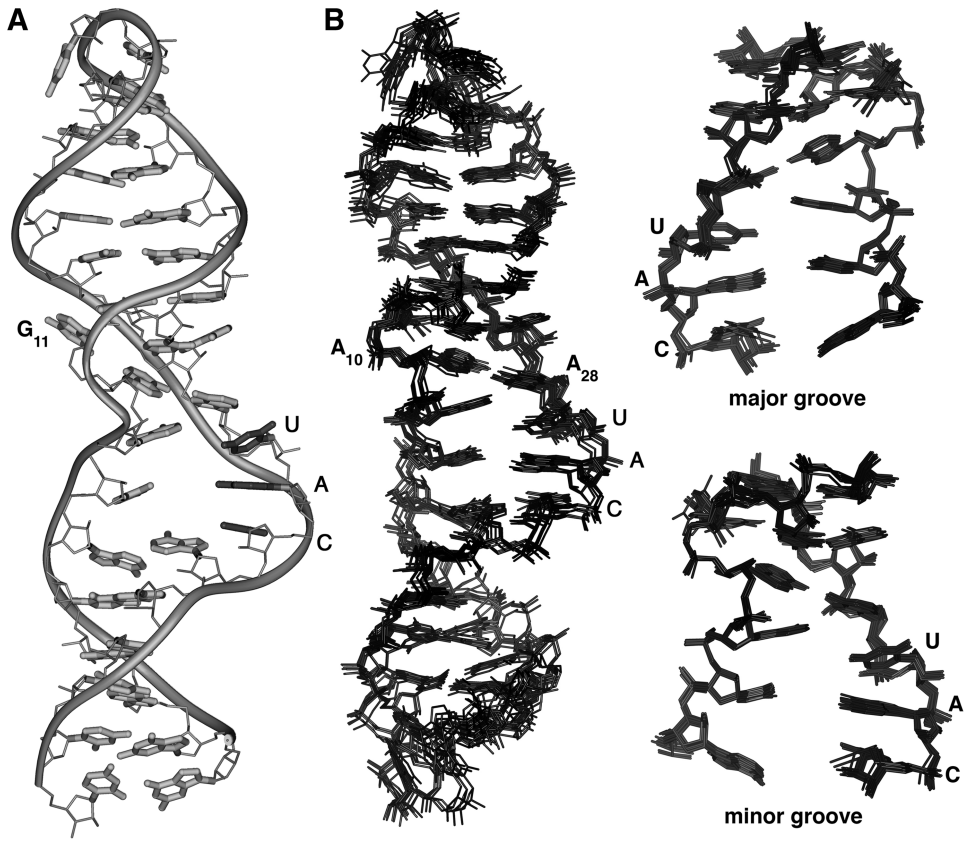

Figure 3. (**A**) Structure of the $tyrS_{SD}$ RNA with view into the minor groove at the center of the helix. (**B**) Superposition of 11 lowest energy structures for the full $tyrS_{SD}$, and the Specifier Loop domain only. Views are into the minor groove at the center of the Specifier Loop domain. The RMSDs between the individual structures and the average structure are listed in Table 1. The internal loop and stem regions are generally well defined. The disorder of the bulged G_{11} base reflects the paucity of constraints for this residue.

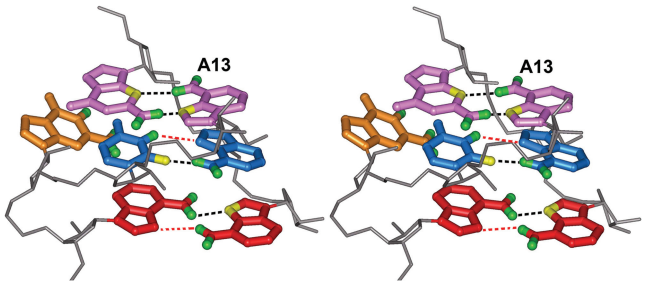

Figure 4. Stereoview of the loop E motif bases in the $tyrS_{SD}$ RNA molecule showing the arrangement of base–base interactions. Hydrogen bonds, supported by ^{15}N chemical shifts, are indicated by dashed black lines. Hydrogen bonds present in other loop E motifs but for which there is no evidence in the $tyrS_{SD}$ RNA are shown as dashed red lines. The sheared G–A base pair (pink), reverse Hoogstein A–U base pair (blue), parallel A–A base pair (red) stack on each other. The bulged G_{11} base (orange) makes no hydrogen bonds with either the phosphate backbone or the flanking bases.

Residues within the Specifier Loop domain of the leader RNA bind directly to the anticodon nucleotides of cognate tRNA molecules and confer specificity to the leader RNA–tRNA interaction. The Specifier Loop domain also contains conserved nucleotides that correspond to the loop E RNA secondary structure motif.

Structure of conserved residues in the *tyrS* leader RNA Specifier Loop domain

The 14 nt corresponding to the Specifier Loop domain of the *B. subtilis tyrS* leader RNA are well ordered and only moderately dynamic. The results show that the nucleotides in the upper half of the domain adopt a loop E motif (Figure 3). This structural element includes an S-turn of the phosphate backbone at residue A_{10} resulting in an inverted orientation of the A_{10} ribose. Although well ordered, the loop E element in the Specifier Loop domain has a more open and possibly more flexible fold than loop E motifs in other contexts (13,17,44). The hydrogen-bonding pattern among the loop E motif bases could be inferred only from ^{15}N chemical shifts and could not be directly confirmed through hydrogen bond-mediated inter-base correlations. These results point to a fold that is open and may be partially accessible to solvent (Figure 5). Flexibility on the intermediate timescale in this region is reflected in the exchange-broadened base resonances of residues G_{11}–A_{13} and the relaxation data support the modest dynamic nature. The limited mobility of these residues may allow for an organized target to be presented to the incoming tRNA anticodon but still allow sufficient flexibility to optimize Specifier Sequence nucleotide–anticodon pairing.

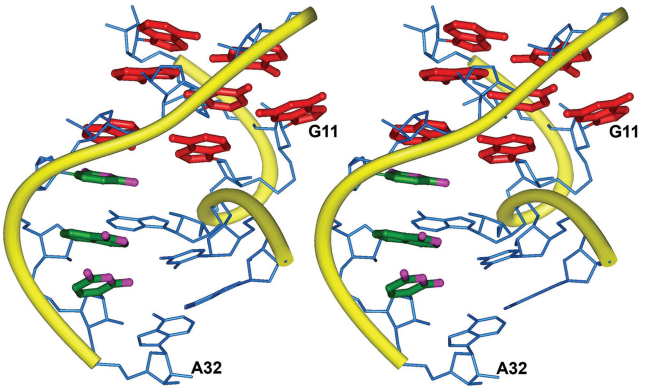

Figure 5. Stereoview of the minimized average structure of the Specifier Loop domain. The specifier nucleotide bases are colored green and the loop E motif nucleotide bases are colored red. The functional groups on the Watson–Crick edges of the specifier nucleotides are colored pink. The S-turn of the sugar-phosphate backbone can be seen between residues A_8 and G_{11}.

To determine if the more open structure results from an insufficient number of experimental constraints, a set of calculations was performed that explicitly imposed base–base interactions present in canonical loop E motifs identified in other studies (13,17,44). The structures calculated using these constraints have approximately twice as many NOE violations (36 per structure) and greater RDC errors (16.6 Hz on average) than the more open structures. Most of the new violations are in the internal loop region and include restraints involving the loop E motif and Specifier Sequence nucleotides. These results support the experimental constraints as the driving force for the more open conformation.

While the upper half of the Specifier Loop domain exhibits extensive cross-strand interactions, nucleotides in the lower half present no evidence for cross-strand pairing. The Specifier Sequence nucleotides maintain regular base stacking with their Watson–Crick edges rotated toward the minor groove (Figure 5). The residue 3′ to the Specifier Sequence, A_{32}, also is single stranded, but does not form a continuous stack with the Specifier Sequence bases. Instead, A_{32}, which pairs with U_{33} of tRNA, stacks on G_{33} of the lower helix. The 5′ strand residues are less well stacked and are slightly rotated toward the major groove. The unpaired nature of this region is consistent with biochemical data that indicate the susceptibility of these nucleotides to Mg^{2+} cleavage (7).

The structure and dynamics of the Specifier Loop domain contrast with those of the 7-nt bulge within the antiterminator hairpin (46). The antiterminator hairpin is one of two mutually exclusive stem–loop structures that can form near the 3′-end of the leader RNA (Figure 1). The antiterminator hairpin contains a bulge of 7 nt, four of which pair with the 3′ terminal nucleotides of uncharged tRNA (4). The three invariant nucleotides (UGG) that pair with tRNA are at the 5′-end of the bulge and display considerable flexibility. These residues appear to sample multiple conformations and do not have a unique structure in the absence of tRNA (46). Nucleotides at the 3′-end of the bulge are highly conserved and well ordered, and are stabilized primarily by base–base stacking. While the flexibility associated with the invariant residues is an important component of their tRNA binding function, the more rigid 3′-end of the bulge may limit the conformations sampled by the loop nucleotides and facilitate tRNA binding (46). The significant dynamics among the tRNA-pairing nucleotides in the antiterminator hairpin is not shared by the Specifier Sequence nucleotides. Although Specifier Sequence–tRNA pairing requires additional rotation of the Specifier Sequence bases away from the helix axis, these residues are well ordered and appear to be stabilized by stacking. The ribose groups of these residues also exhibit limited dynamics and adopt the regular A-form 3′-*endo* conformation. The three residues of the Specifier Loop domain that are dynamic (G_{11}–A_{13}) may provide flexibility to optimize tRNA binding.

Role of the loop E motif in tRNA binding

The loop E motif is a common RNA structural element that is well represented in ribosomal RNAs (13,37,47–50), loop B of the hairpin ribozyme (15,51), the specificity domains of some type B RNase P molecules (52,53), the internal ribosome entry site (IRES) element found in the 5′ untranslated region of hepatitis C virus (HCV) RNA (54,55), the central domain of potato spindle tuber viroid (PSTV) (37), and in *in vitro* selected nucleolin recognition element (sNRE) mutants (17). Loop E nucleotides participate directly in protein–RNA interactions in most of the rRNA molecules and in the sNRE RNA (13,16,17,47,49,56) and, in the hairpin ribozyme, the motif forms part of a corridor for active site water migration (57). In the case of the loop E structures found in domains IIb and IIId of the IRES element of HCV RNA, it is still not clear whether the loop E structure provides a platform for protein or RNA binding (54,55).

The functional importance of the loop E motif in the Specifier Loop domain is suggested by nucleotide conservation and mutagenesis (11, Green,N.J., Grundy,F.J. and Henkin,T.M., unpublished data). Comparison of the Specifier Loop domains of several T-box leader RNAs across multiple bacterial species shows the conservation of two elements, the Specifier Sequence nucleotides at the 3′ end of the 3′ strand followed by an unpaired adenine nucleotide and a group of 7 nt in the upper part of the internal loop that correspond to the loop E motif (11,58). The number and identities of the remaining nucleotides in the Specifier Loop domain are variable, but nucleotide changes within the loop E motif can be deleterious. For example, an uridine-to-cytidine mutation in the Specifier Loop domain of the *glyQS* leader RNA at a position corresponding to residue 12 in the $tyrS_{SD}$ RNA leads to loss of function in *in vivo* and *in vitro* transcriptional attenuation assays (Green,N.J., Grundy,F.J. and Henkin,T.M., unpublished data). Figure 6 shows that resonances primarily affected by the U-to-C mutation correspond to nucleotides that comprise the loop E motif and indicate that the structure of the motif has been disrupted. Interestingly, the structural

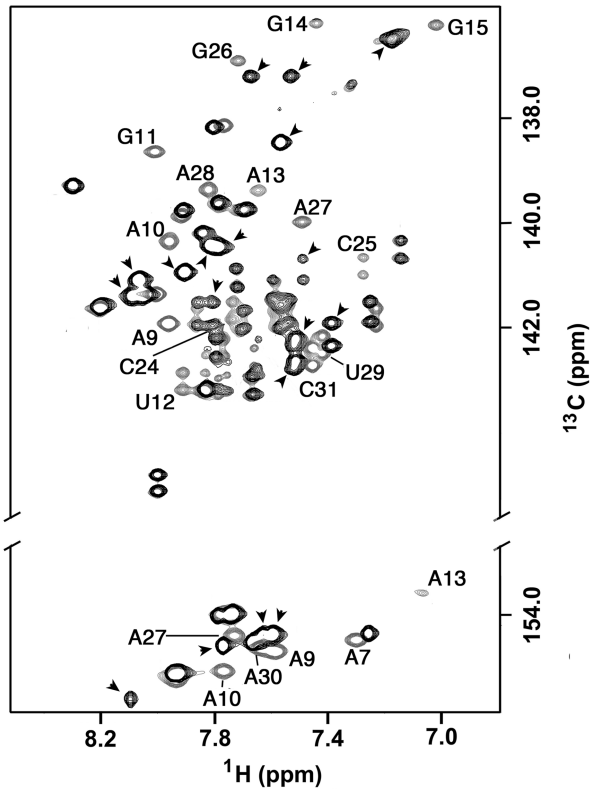

Figure 6. Overlay of the base C6/8 and C2 regions of ^{13}C-^{1}H HSQC spectra of $tyrS_{SD}$ RNA molecule (gray) and the $tyrS_{SD}$ RNA molecule with the substitution U_{12} to C_{12} (black). Peaks from the native sequence shifted by the mutation are labeled. Peaks from the sequence containing the $U_{12}C$ mutation that do not overlap peaks from the native sequence are indicated by an arrow. The resonances most affected by the single base substitution correspond to the residues of the loop E motif. Nucleotides in the opposite end of the internal loop, including specifier nucleotides A_{30} and C_{31} show much smaller affects.

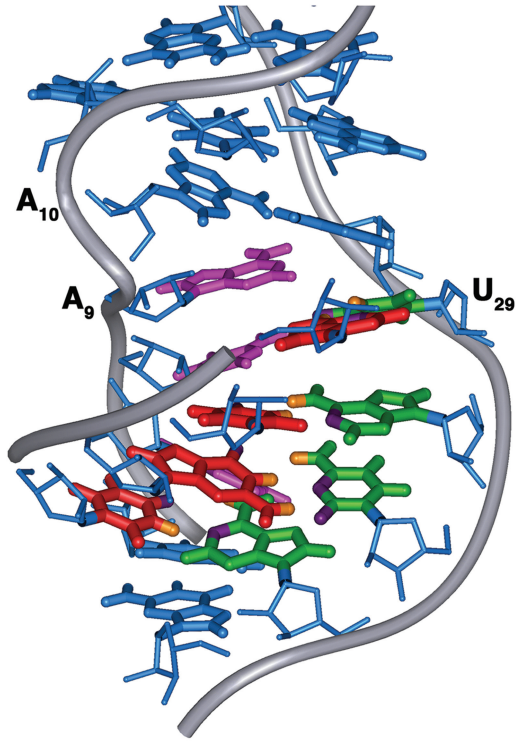

Figure 7. Proposed model of the interaction between the Specifier Loop domain and the tRNA anticodon loop. Nucleotide bases in the anticodon loop (red) approach from the minor groove side of the Specifier Domain and form Watson–Crick base pairs with the Specifier Sequence bases (green). Nucleotides of the partner strand (pink) rotate toward the major groove. The S-turn of the phosphate backbone on the partner strand is introduced by the loop E motif (blue) and facilitates the minor groove displacement of the Specifier Sequence bases.

perturbations appear limited to the loop E motif. The chemical shifts corresponding to the residues of the Specifier Loop domain outside of the loop E motif are not significantly affected by the mutation, suggesting minimal perturbation of their local structure.

The structure of $tyrS_{SD}$ and the effects caused by the U-to-C mutation suggest a model for tRNA binding to the Specifier Sequence on the minor groove side of the Specifier Loop domain (Figure 7). The Specifier Sequence bases are well ordered in the solution structure and are only moderately more dynamic than the helix residues, suggesting that they are primed for pairing with the tRNA anticodon loop. In order for the Specifier Sequence nucleotides to pair with tRNA, the bases must rotate out toward the major or minor groove to present their Watson–Crick edges. Rotation toward the major groove would result in under-winding of the sugar-phosphate backbone, whereas rotation toward the minor groove would entail over-winding of the backbone. In the structure of $tyrS_{SD}$, the 4 Specifier Sequence bases turn toward the minor groove, whereas the 3 bases of the partner strand turn out toward the major groove.

We propose that the S-turn of the loop E motif is responsible for this base positioning and that it acts through the phosphate backbone. The S-turn, centered on A_{10}, causes a differential shortening of the distance between the lower helix and the A_{10}–A_{28} base pair of the loop. To accommodate the constraints on the phosphate backbone imposed by the S-turn and the asymmetric number of residues in this region, bases on the partner strand rotate toward the major groove and the Specifier Sequence bases rotate toward the minor groove. Although the U-to-C mutation does not appear to affect the local structure around the Specifier Sequence nucleotides, their propensity to rotate toward the minor groove would be impaired by loss of the S-turn at A_{10}. Thus, in this model for tRNA binding, the loop E motif positions a specific structural component, the S-turn, that kinks the sugar-phosphate backbone of the partner strand and promotes rearrangement of the Specifier Sequence bases toward the minor groove for pairing with the tRNA (Figure 7). The loop E motif may additionally provide a platform to help stabilize the duplex formed by the Specifier Sequence and anticodon base pairs through stacking interactions.

ACCESSION NUMBER

Atomic coordinates for the refined structures have been deposited with the Protein Data Bank under accession code 2KHY.

SUPPLEMENTARY DATA

Supplementary Data are available at NAR Online.

ACKNOWLEDGEMENTS

We thank Malgorzata Michnicka for preparation of the T7 RNA polymerase and synthesis of the labeled 5′-nucleotide triphosphates. The 800 MHz NMR spectrometer was purchased with funds from the W. M. Keck Foundation and the John S. Dunn Foundation.

FUNDING

The Robert A. Welch Foundation (C-1277 to E.P.N.) and by the National Institutes of Health (GM73969 to E.P.N.; GM47823 to T.M.H.). Funding for open access charge: National Institutes of Health.

Conflict of interest statement. None declared.

REFERENCES

1. Henkin,T.M. (2008) Riboswitch RNAs: using RNA to sense cellular metabolism. *Genes Dev.*, **22**, 3383–3390.
2. Henkin,T.M. and Grundy,F.J. (2006) Sensing metabolic signals with nascent RNA transcripts: the T box and S box riboswitches as paradigms. *Cold Spring Harbor Symp. Quant. Biol.*, **71**, 231–237.
3. Grundy,F.J. and Henkin,T.M. (1993) tRNA as a positive regulator of transcription antitermination in *B. subtilis*. *Cell*, **74**, 475–482.
4. Grundy,F.J., Rollins,S.M. and Henkin,T.M. (1994) Interaction between the acceptor end of tRNA and the T box stimulates antitermination in the *Bacillus subtilis tyrS* gene: a new role for the discriminator base. *J. Bacteriol.*, **176**, 4518–4526.
5. Grundy,F.J., Hodil,S.E., Rollins,S.M. and Henkin,T.M. (1997) Specificity of tRNA-mRNA interactions in *Bacillus subtilis tyrS* antitermination. *J. Bacteriol.*, **179**, 2587–2594.
6. Grundy,F.J., Moir,T.R., Haldeman,M.T. and Henkin,T.M. (2002a) Sequence requirements for terminators and antiterminators in the T box transcription antitermination system: disparity between conservation and functional requirements. *Nucleic Acids Res.*, **30**, 1646–1655.
7. Yousef,M.R., Grundy,F.J. and Henkin,T.M. (2005) Structural transitions induced by the interaction between $tRNA^{Gly}$ and the *Bacillus subtilis glyQS* T box leader RNA. *J. Mol. Biol.*, **349**, 273–287.
8. Grundy,F.J. and Henkin,T.M. (1994) Conservation of a transcription antitermination mechanism in aminoacyl-tRNA synthetase and amino acid biosynthesis genes in Gram-positive bacteria. *J. Mol. Biol.*, **235**, 798–804.
9. Grundy,F.J., Winkler,W.C. and Henkin,T.M. (2002b) tRNA-mediated transcription antitermination *in vitro*: codon-anticodon pairing independent of the ribosome. *Proc. Natl Acad. Sci. USA*, **99**, 11121–11126.
10. Nelson,A.R., Henkin,T.M. and Agris,P.F. (2006) tRNA regulation of gene expression: interactions of an mRNA 5′-UTR with a regulatory tRNA. *RNA*, **12**, 1254–1261.
11. Rollins,S.M., Grundy,F.J. and Henkin,T.M. (1997) Analysis of *cis*-acting sequence and structural elements required for antitermination of the *Bacillus subtilis tyrS* gene. *Mol. Microbiol.*, **25**, 411–421.
12. Szewczak,A.A. and Moore,P.B. (1995) The sarcin/ricin loop, a modular RNA. *J. Mol. Biol.*, **247**, 81–98.
13. Dallas,A. and Moore,P.B. (1997) The loop E-loop D region of *Escherichia coli* 5S rRNA: the solution structure reveals an unusual loop that may be important for binding ribosomal proteins. *Structure*, **5**, 1639–1653.
14. Leontis,N.B. and Westhof,E. (1998) A common motif organizes the structure of multi-helix loops in 16 S and 23 S ribosomal RNAs. *J. Mol. Biol.*, **283**, 571–583.
15. Butcher,S.E. and Burke,J.M. (1994a) A photo-cross-linkable tertiary structure motif found in functionally distinct RNA molecules is essential for catalytic function of the hairpin ribozyme. *Biochemistry*, **33**, 992–999.
16. Bouvet,P., Allain,F.H., Finger,L.D., Dieckmann,T. and Feigon,J. (2001) Recognition of pre-formed and flexible elements of an RNA stem-loop by nucleolin. *J. Mol. Biol.*, **309**, 763–775.
17. Johansson,C., Finger,L.D., Trantirek,L., Mueller,T.D., Kim,S., Laird-Offringa,I.A. and Feigon,J. (2004) Solution structure of the complex formed by the two N-terminal RNA-binding domains of nucleolin and a pre-rRNA target. *J. Mol. Biol.*, **337**, 799–816.
18. Brunel,C., Romby,P., Westhof,E., Ehresmann,C. and Ehresmann,B. (1991) Three-dimensional model of *Escherichia coli* ribosomal 5 S RNA as deduced from structure probing in solution and computer modeling. *J. Mol. Biol.*, **221**, 293–308.
19. Davanloo,P., Rosenberg,A.H., Dunn,J.J. and Studier,F.W. (1984) Cloning and expression of the gene for bacteriophage T7 RNA polymerase. *Proc. Natl Acad. Sci. USA*, **81**, 2035–2039.
20. Milligan,J.F., Groebe,D.R., Witherell,G.W. and Uhlenbeck,O.C. (1987) Oligoribonucleotide synthesis using T7 RNA polymerase and synthetic DNA templates. *Nucleic Acids Res.*, **15**, 8783–8798.
21. Nikonowicz,E.P., Sirr,A., Legault,P., Jucker,F.M., Baer,L.M. and Pardi,A. (1992) Preparation of ^{13}C and ^{15}N labelled RNAs for heteronuclear multi-dimensional NMR studies. *Nucleic Acids Res.*, **20**, 4507–4513.
22. Hansen,M.R., Mueller,L. and Pardi,A. (1998) Tunable alignment of macromolecules by filamentous phage yields dipolar coupling interactions. *Nat. Struct. Biol.*, **5**, 1065–1074.
23. Marino,J.P., Diener,J.L., Moore,P.B. and Griesinger,C. (1997) Multiple-quantum Coherence dramatically enhances the sensitivity of CH and CH_2 correlations in uniformly ^{13}C-labeled RNA. *J. Am. Chem. Soc.*, **119**, 7361–7366.
24. Schwieters,C.D., Kuszewski,J.J., Tjandra,N. and Clore,G.M. (2003) The Xplor-NIH NMR molecular structure determination package. *J. Magn. Reson.*, **160**, 65–73.
25. Dingley,A.J. and Grzesiek,S. (1998) Direct observation of hydrogen bonds in nucleic acid base pairs by internucleotide $^{2}J_{NN}$ couplings. *J. Am. Chem. Soc.*, **120**, 8293–8297.
26. Varani,G., Aboul-ela,F. and Allain,F.H.T. (1996) NMR investigation of RNA structure. *Prog. Nucl. Magn. Reson. Spec.*, **29**, 51–127.
27. Szep,S., Wang,J. and Moore,P.B. (2003) The crystal structure of a 26-nucleotide RNA containing a hook-turn. *RNA*, **9**, 44–51.
28. Correll,C.C., Freeborn,B., Moore,P.B. and Steitz,T.A. (1997) Metals, motifs, and recognition in the crystal structure of a 5S rRNA domain. *Cell*, **91**, 705–712.
29. Gorenstein,D.G. (1984) *Phosphorus-31 NMR: Principles and Applications*. Academic Press, New York.
30. Clore,G.M. and Kuszewski,J. (2003) Improving the accuracy of NMR structures of RNA by means of conformational database potentials of mean force as assessed by complete dipolar coupling cross-validation. *J. Am. Chem. Soc.*, **125**, 1518–1525.
31. Simorre,J.-P., Zimmermann,G.R., Mueller,L. and Pardi,A. (1996) Triple-resonance experiments for assignment of adenine base resonances in $^{13}C/^{15}N$-labeled RNA. *J. Am. Chem. Soc.*, **118**, 5316–5317.
32. Pardi,A. (1995) Multidimensional heteronuclear NMR experiments for structure determination of isotopically labeled RNA. *Methods Enzymol.*, **261**, 350–380.
33. Dieckmann,T. and Feigon,J. (1997) Assignment methodology for larger RNA oligonucleotides: application to an ATP-binding RNA aptamer. *J. Biomol. NMR*, **9**, 259–272.
34. Allain,F.H.-T. and Varani,G. (1995) Divalent metal ion binding to a conserved wobble pair defining the upstream site of cleavage of group I self-splicing introns. *Nucleic Acids Res.*, **23**, 341–350.
35. Heus,H.A., Wijmenga,S.S., van de Ven,F.J.M. and Hilbers,C.W. (1994) Sequential backbone assignment in ^{13}C-labeled RNA via through-bond coherence transfer using three-dimensional triple resonance spectroscopy (^{1}H,^{13}C,^{31}P) and two-dimensional hetero TOCSY. *J. Am. Chem. Soc.*, **116**, 4983–4984.

36. Kellogg,G.W. and Schweitzer,B.I. (1993) Two- and three-dimensional ^{31}P-driven NMR procedures for complete assignment of backbone resonances in oligodeoxyribonucleotides. *J. Biomol. NMR*, **3**, 577–595.
37. Branch,A.D., Benenfeld,B.J. and Robertson,H.D. (1985) Ultraviolet light-induced crosslinking reveals a unique region of local tertiary structure in potato spindle tuber viroid and HeLa 5S RNA. *Proc. Natl Acad. Sci. USA*, **82**, 6590–6594.
38. Butcher,S.E. and Burke,J.M. (1994b) Structure-mapping of the hairpin ribozyme. Magnesium-dependent folding and evidence for tertiary interactions within the ribozyme-substrate complex. *J. Mol. Biol.*, **244**, 52–63.
39. Tolbert,B.S., Kennedy,S.D., Schroeder,S.J., Krugh,T.R. and Turner,D.H. (2007) NMR structures of $(rGCUGAGGCU)_2$ and $(rGCGGAUGCU)_2$: probing the structural features that shape the thermodynamic stability of GA pairs. *Biochemistry*, **46**, 1511–1522.
40. Serra,M.J., Baird,J.D., Dale,T., Fey,B.L., Retatagos,K. and Westhof,E. (2002) Effects of magnesium ions on the stabilization of RNA oligomers of defined structures. *RNA*, **8**, 307–323.
41. Butcher,S.E., Allain,F.H. and Feigon,J. (2000) Determination of metal ion binding sites within the hairpin ribozyme domains by NMR. *Biochemistry*, **39**, 2174–2182.
42. Rupert,P.B. and Ferre-D'Amare,A.R. (2001) Crystal structure of a hairpin ribozyme-inhibitor complex with implications for catalysis. *Nature*, **410**, 780–786.
43. Finger,L.D., Trantirek,L., Johansson,C. and Feigon,J. (2003) Solution structures of stem-loop RNAs that bind to the two N-terminal RNA-binding domains of nucleolin. *Nucleic Acids Res.*, **31**, 6461–6472.
44. Correll,C.C., Wool,I.G. and Munishkin,A. (1999) The two faces of the *Escherichia coli* 23 S rRNA sarcin/ricin domain: the structure at 1.11 Å resolution. *J. Mol. Biol.*, **292**, 275–287.
45. Grundy,F.J., Collins,J.A., Rollins,S.M. and Henkin,T.M. (2000) tRNA determinants for transcription antitermination of the *Bacillus subtilis tyrS* gene. *RNA*, **6**, 1131–1141.
46. Gerdeman,M.S., Henkin,T.M. and Hines,J.V. (2003) Solution structure of the *Bacillus subtilis* T-box antiterminator RNA: seven nucleotide bulge characterized by stacking and flexibility. *J. Mol. Biol.*, **326**, 189–201.
47. Ban,N., Nissen,P., Hansen,J., Moore,P.B. and Steitz,T.A. (2000) The complete atomic structure of the large ribosomal subunit at 2.4 Å resolution. *Science*, **289**, 905–920.
48. Endo,Y., Gluck,A. and Wool,I.G. (1993) Ribosomal RNA identity elements for recognition by ricin and by alpha-sarcin: mutation in the putative CG pair that closes a GAGA tetraloop. *Nucleic Acids Symp Ser.*, **29**, 165–166.
49. Schuwirth,B.S., Borovinskaya,M.A., Hau,C.W., Zhang,W., Vila-Sanjurjo,A., Holton,J.M. and Cate,J.H. (2005) Structures of the bacterial ribosome at 3.5 Å resolution. *Science*, **310**, 827–834.
50. Wimberly,B., Varani,G. and Tinoco,I. Jr (1993) The conformation of loop E of eukaryotic 5S ribosomal RNA. *Biochemistry*, **32**, 1078–1087.
51. Butcher,S.E., Allain,F.H. and Feigon,J. (1999) Solution structure of the loop B domain from the hairpin ribozyme. *Nat. Struct. Biol.*, **6**, 212–216.
52. Krasilnikov,A.S., Yang,X., Pan,T. and Mondragon,A. (2003) Crystal structure of the specificity domain of ribonuclease P. *Nature*, **421**, 760–764.
53. Massire,C., Jaeger,L. and Westhof,E. (1998) Derivation of the three-dimensional architecture of bacterial ribonuclease P RNAs from comparative sequence analysis. *J. Mol. Biol.*, **279**, 773–793.
54. Klinck,R., Westhof,E., Walker,S., Afshar,M., Collier,A. and Aboul-Ela,F. (2000) A potential RNA drug target in the hepatitis C virus internal ribosomal entry site. *RNA*, **6**, 1423–1431.
55. Lukavsky,P.J., Kim,I., Otto,G.A. and Puglisi,J.D. (2003) Structure of HCV IRES domain II determined by NMR. *Nat. Struct. Biol.*, **10**, 1033–1038.
56. Selmer,M., Dunham,C.M., Murphy,F.V.t., Weixlbaumer,A., Petry,S., Kelley,A.C., Weir,J.R. and Ramakrishnan,V. (2006) Structure of the 70S ribosome complexed with mRNA and tRNA. *Science*, **313**, 1935–1942.
57. Salter,J., Krucinska,J., Alam,S., Grum-Tokars,V. and Wedekind,J.E. (2006) Water in the active site of an all-RNA hairpin ribozyme and effects of Gua8 base variants on the geometry of phosphoryl transfer. *Biochemistry*, **45**, 686–700.
58. Gutierrez-Preciado,A., Henkin,T.M., Grundy,F.J., Yanofsky,C. and Merino,E. (2009) Biochemical features and functional implications of the RNA-based T box regulatory mechanism. *Microbiol. Mol. Biol. Rev.*, **73**, 36–61.
59. Varani,G., Cheong,C. and Tinoco,I. Jr (1991) Structure of an unusually stable RNA hairpin. *Biochemistry*, **30**, 3280–3289.